11th World Congress on Computational Mechanics (WCCM XI)
5th European Conference on Computational Mechanics (ECCM V)
6th European Conference on Computational Fluid Dynamics (ECFD VI)
E. Oñate, J. Oliver and A. Huerta (Eds)

FAILURE OF RC SLABS MODELLED USING AN EMBEDDED DISCONTINUITY APPROACH

GELACIO JUÁREZ-LUNA [*] AND A GUSTAVO AYALA [†]

[*] Departamento de Materiales
Universidad Autónoma Metropolitana
San Pablo 180, Col. Reynosa Tamaulipas, 02200 Azcapotzalco, México City,
e-mail: gjl@azc.uam.mx, http://posgradoscbi.azc.uam.mx/estructuras.php

[†] Instituto de Ingeniería, Universidad Nacional Autónoma de México
Edificio C1, Campus Norte UPC
Ciudad Universitaria 3000, Coyoacán, México, D.F., 04510
email: gayalam@iingen.unam.mx, www.iingen.unam.mx

Key Words: *Slabs, Embedded discontinuities, Damage.*

Abstract. This paper investigates the collapse evolution process of reinforced concrete slabs subject to vertical loading. Concrete was discretized with hexahedral finite elements with embedded discontinuities with three degrees of freedom per node, whereas steel reinforcement was represented by 3D bar elements placed along the borders of the solid elements. This coupling of solid and bar finite elements was validated with a reinforced concrete slab reported in the literature; other two slabs were also investigated showing the cracking patter at the top and the bottom surfaces.

1 INTRODUCTION

The study of collapse in concrete elements is an interest topic in civil engineering, particularly the determination of the magnitude load, which cracking starts and its growth. As it is well known in concrete, cracking starts in zones with stress states under tension before in zones with compression stress states, because the strength magnitude in compression is from 10 to 20 times greater than in tension as shown in the experimental results reported by [24]. In the way to collapse of reinforced concrete elements, their behavior at the beginning is approximately linear elastic; then, cracking starts and finally, plasticity in reinforcing steel occurs. Particularly in clamped reinforced concrete slabs, cracking starts on the top surface, then at the center on the bottom surface, growing as the load increases; whereas in simple supported slabs, cracking starts at the center of the span on the bottom surface, growing to the borders [22].

There are laboratory test to obtain the cracking paths and the moment coefficients of the rectangular slabs such as [4], who tested 52 simple supported on their borders and 35 strips supported as beams, which were loaded until failure occurs. In these experimental tests, the displacements at some points of the slabs and the slopes at the center of the borders were

obtained; also, the propagation of the crack was registered as it is reported by [37]. Afterwards, other experimental test were performed as the reported by [28], [15], [16], [34], [11], [18], [13],[9], [5] and [10], among others. It is interested to say that these references are the base of the research and applications of the current analysis and design of the rectangular slabs.

For the modeling of the reinforced concrete slabs, [7] applied the smear cracking model to study an axisymmetric slab under shear penetration, showing that cracking started at the bottom of the slab and the cracking paths. Then, [25] modeled a square slab supported on its corner with a concentrated load at the center of the span, they obtained the load vs. displacement curve, which was congruent with experimental results reported by [29] and [19]; in the results by [25], neither the start of the cracking nor the cracking path was given. There other proposals for modeling reinforced concrete slabs such as [14], [26], [12], [17], [35], among others.

The are some commercial software for modeling reinforced concrete elements such as ANSYS [3], DIANA [8], ATENA [23], ABAQUS [1], NLFEAS [32], among others. Those software mainly use the finite element method with the smear cracking model for the behavior of the concrete, equipped with a failure surface with different threshold value in tension and compression, necessary to determine the start and propagation of cracking. However, the smear cracking model has numerical problems of stress locking and spurious kinematic modes [30], which are overcome with heuristic shear retention factors.

In this paper, the embedded discontinuity model is applied for studying collapse of reinforced concrete slabs, computing the load, which cracking started, and the cracking patterns. Concrete was discretized with hexahedral finite elements with embedded discontinuities and steel reinforcement was discretized with 3D bar elements, both kinds of elements have three degrees of freedom per node.

2 EMBEDDED DISCONTINUITY MODEL

2.1 Variational formulation

The finite elements with embedded discontinuities are based on a displacement functional [2][20][27][36], given as:

$$\Pi\left(\mathbf{u},\left[\left|\mathbf{u}\right|\right]\right)=\int_{\Omega\setminus S}\left[\Psi(\bar{\boldsymbol{\varepsilon}}^{u})-\mathbf{b}\cdot\mathbf{u}\right]d\Omega-\int_{\Gamma_{\sigma}}\mathbf{t}^{*}\cdot\mathbf{u}\,d\Gamma+\int_{\Gamma_{S}}\phi_{S}(\left[\left|\mathbf{u}\right|\right])d\Gamma \tag{1}$$

where the free energy density, $\Psi(\bar{\boldsymbol{\varepsilon}}^{u})$, depends on the continuous strain field $\bar{\boldsymbol{\varepsilon}}$, and the free discrete energy density, $\Psi_{S}(\left[\left|\mathbf{u}\right|\right])$, depends on the jump given by:

$$\Psi(\bar{\boldsymbol{\varepsilon}})=\int_{0}^{\bar{\boldsymbol{\varepsilon}}}\boldsymbol{\sigma}(\bar{\boldsymbol{\varepsilon}})\,d\bar{\boldsymbol{\varepsilon}} \tag{2}$$

$$\phi_{S}(\left[\left|\mathbf{u}\right|\right])=\int_{0}^{[|\mathbf{u}|]}\mathbf{T}_{S}(\left[\left|\mathbf{u}\right|\right]_{n,s})\,d\left[\left|\mathbf{u}\right|\right] \tag{3}$$

which the elastic stress, $\boldsymbol{\sigma}$, is defined by:

$$\boldsymbol{\sigma}=\mathbf{C}\;:\;\bar{\boldsymbol{\varepsilon}} \tag{4}$$

2.2 Finite element approximation

It is not possible to prescribe the boundary conditions, $\mathbf{u}^*$, in only one of the displacement fields, *i.e.*, $\bar{\mathbf{u}}$ or [|**u**|], a difficulty overcame, according to [21], defining the displacement as in Eq. (5) shown in Figures 1**Figure 1**a and b:

$$\mathbf{u} = \hat{\mathbf{u}} + M_S(\mathbf{x})\left[\left|\mathbf{u}\right|\right] \tag{5}$$

Then, the strain field is defined by:

$$\boldsymbol{\varepsilon} = \nabla^S \mathbf{u} = \nabla^S \hat{\mathbf{u}} + \nabla^S M_S(\mathbf{x})\left[\left|\mathbf{u}\right|\right] \tag{6}$$

where $\hat{\mathbf{u}}$ is the regular displacement field and $M_S(\mathbf{x})$ is a function given by:

$$M_S(\mathbf{x}) = H_S(\mathbf{x}) - \phi(\mathbf{x}) \tag{7}$$

Where $\phi(\mathbf{x})$ is a continuous function such that:

$$\begin{aligned} \phi(\mathbf{x}) &= 0 \quad \forall \mathbf{x} \in \Omega^- \\ \phi(\mathbf{x}) &= 1 \quad \forall \mathbf{x} \in \Omega^+ \end{aligned} \tag{8}$$

The function M_S, has two properties: $M_S(x) = 1 \quad \forall x \in S$ and $M_S(x) = 0 \quad \forall x \in \Omega^- \cup \Omega^+$ as shown in Figure 1.

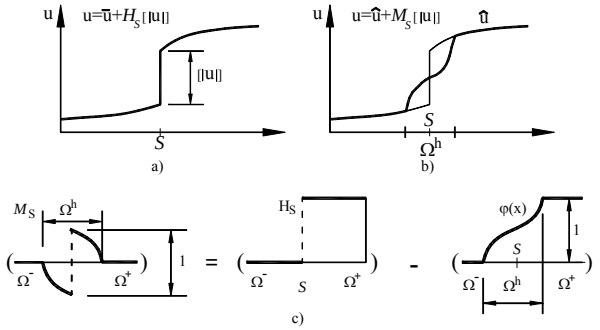

Figure 1: Graphic representation of : a) continuus, b) regular displacements and c) function M_S.

The continuous displacement field is defined as:

$$\bar{\mathbf{u}} = \hat{\mathbf{u}} - \phi(\mathbf{x})\left[\left|\mathbf{u}\right|\right] \tag{9}$$

In the continuous part of the solid, which may be linear elastic, the continuous strain field, $\bar{\boldsymbol{\varepsilon}}$ is given by:

$$\bar{\boldsymbol{\varepsilon}} = \nabla^S \bar{\mathbf{u}} \tag{10}$$

Substituting Eq. (9) into Eq. (10),

$$\bar{\boldsymbol{\varepsilon}} = \nabla^S \hat{\mathbf{u}} - \nabla^S \phi(\mathbf{x})\left[\left|\mathbf{u}\right|\right] - \phi(\mathbf{x})\nabla^S\left[\left|\mathbf{u}\right|\right] \tag{11}$$

If the displacement jump is constant in Eq. (11), the continuous strain field may be rewritten as:

$$\bar{\boldsymbol{\varepsilon}} = \nabla^S \hat{\mathbf{u}} - \nabla^S \phi(\mathbf{x})\left[\left|\mathbf{u}\right|\right] \tag{12}$$

2.3 Approximation of the displacement and strain fields

The regular displacement field is approximated by:

$$\hat{\mathbf{u}} = \mathbf{Nd} \tag{13}$$

where $\mathbf{N}$ is the standard vector of shape functions of the element

$$\mathbf{N} = \sum_{i=1}^{i=n} N_i^{(e)} \tag{14}$$

and, $\mathbf{d}$, is the nodal displacement vector. The function, $M_S(\mathbf{x})$, is defined in the finite element approximation as:

$$M_S^e(\mathbf{x}) = H_S^e(\mathbf{x}) - \phi^e \tag{15}$$

where ϕ^e is constructed by:

$$\phi^e = \sum_{i^+=1}^{n_e^+} N_{i^+} \tag{16}$$

where N_{i^+} are the shape functions corresponding to the nodes placed on Ω^+ of the finite element which contains the discontinuity, in agreement with the definition of ϕ in Eq. (8).

The displacement field defined in Eq. (5) is given by

$$\mathbf{u} = \mathbf{Nd} + \underbrace{M_S^e}_{\mathbf{N}_c} \left[\left|\mathbf{u}\right|\right]_{x,y} \tag{17}$$

The continuous strain field in Eq. (12) is approximated as:

$$\bar{\boldsymbol{\varepsilon}} = \mathbf{B} \cdot \mathbf{d} - \underbrace{\nabla \phi^e}_{\mathbf{B}_c} \cdot \left[\left|\mathbf{u}\right|\right]_{x,y} \quad \forall \mathbf{x} \in \Omega \,/\, S \tag{18}$$

where $\mathbf{B}$, is the standard strain interpolation matrix, containing the derivatives of the standard shape functions $\partial(\mathbf{Nd}) = \mathbf{Bd}$.

The equilibrium equations corresponding to this formulation are obtained by substituting Eqs. (17) and (18) into the energy functional of Eq. (1), and setting the derivatives with respect to the variables ($\mathbf{d}$ and $[|\mathbf{u}|]$) to zero,

$$\frac{\partial \Pi}{\partial \mathbf{d}} = 0 = \int_{\Omega \setminus S} \mathbf{B}^T \boldsymbol{\sigma}\left(\bar{\boldsymbol{\varepsilon}}\right) d\Omega - \int_{\Omega} \mathbf{N}^T \cdot \mathbf{b}\, d\Omega - \int_{\Gamma_\sigma} \mathbf{N}^T \cdot \mathbf{t}^* d\Gamma \tag{19}$$

$$\frac{\partial \Pi}{\partial \left[\left|\mathbf{u}\right|\right]} = 0 = -\int_{\Omega \setminus S} \mathbf{B}_c^T \boldsymbol{\sigma}\left(\bar{\boldsymbol{\varepsilon}}\right) d\Omega + \int_{\Gamma_S} \mathbf{T}_{x,y} d\Gamma \tag{20}$$

As in Eqs. (19) and (20), $\boldsymbol{\sigma}\left(\bar{\boldsymbol{\varepsilon}}\right)$ and $\mathbf{T}_{x,y,z}$ are nonlinear, their respective linearizations with Taylor series give [21]:

$$\begin{bmatrix} \int_{\Omega \setminus S} \mathbf{B}^{\mathbf{T}} \cdot \mathbf{C} \cdot \mathbf{B}\, d\Omega & -\int_{\Omega \setminus S} \mathbf{B}^{\mathbf{T}} \cdot \mathbf{C} \cdot \mathbf{B}_c\, d\Omega \\ -\int_{\Omega \setminus S} \mathbf{B}_c^{\mathbf{T}} \cdot \mathbf{C} \cdot \mathbf{B}\, d\Omega & -\int_{\Omega \setminus S} \mathbf{B}_c^{\mathbf{T}} \cdot \mathbf{C} \cdot \mathbf{B}_c\, d\Omega + \int_{\Gamma_S} \mathbf{R}^T \cdot \mathbf{T} \cdot \mathbf{R}\, d\Gamma \end{bmatrix}^{(n,0)} \begin{Bmatrix} \Delta d \\ \Delta\left[\left|\mathbf{u}\right|\right]_{x,y} \end{Bmatrix}^{(n,1)} = \begin{Bmatrix} R_1 \\ R_2 \end{Bmatrix}^{(n,0)} \tag{21}$$

where $\mathbf{R}$ has the direction cosines, R_1 and R_2 are defined as:

$$R_1 = F_{ext}^{(n)} - \int_{\Omega \setminus S} \mathbf{B}^T \boldsymbol{\sigma}\left(\bar{\boldsymbol{\varepsilon}}\right) d\Omega^{(n,0)} \tag{22}$$

$$R_2 = \int_{\Omega \setminus S} \mathbf{B}_c^T \boldsymbol{\sigma}\left(\bar{\boldsymbol{\varepsilon}}\right) d\Omega^{(n,0)} - \int_{\Gamma_S} \mathbf{T}_{x,y} d\Gamma^{(n,0)} \tag{23}$$

To reduce the size of the system given in Eq. (21), the additional degree of freedom, $\Delta[|\mathbf{u}|]$, may be condensed. In Eq. (22), R_1 means the equilibrium between the external and the internal forces in the domain $\Omega \setminus S$, whereas R_2, in Eq. (23), the equilibrium between the forces in the domain $\Omega \setminus S$ and forces in the discontinuity Γ_S.

Tractions at the discontinuity are:

$$\mathbf{T}_{x,y,z} = \frac{1}{A_d} \int_{\Omega \setminus S} \mathbf{B}_c^T \boldsymbol{\sigma} d\Omega \tag{24}$$

which expressed in the local system becomes

$$\mathbf{T}_{n,s,t} = \frac{1}{A_d} \mathbf{R} \int_{\Omega \setminus S} \mathbf{B}_c^T \boldsymbol{\sigma} d\Omega \tag{25}$$

The definitions of the traction vector in Eqs. (24) and (25) are dependent on the discontinuity area, A_d, and the direction cosines to the normal vector **n**, as shown in Figure 2.

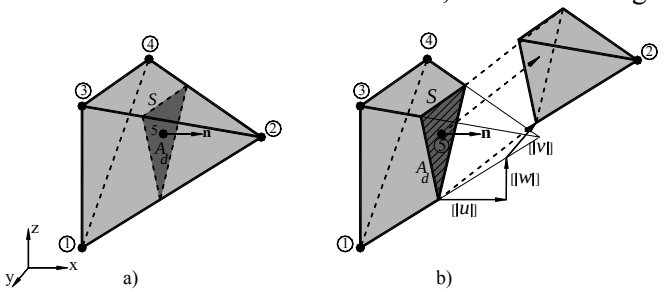

Figure 2: Finite element: a) discontinuity area and b) displacement jumps

This finite element with embedded discontinuity was implemented in the finite element analysis program (FEAP) [33]. This element capture a discontinuity surface at is geometric center, the discontinuity surfaces between surrounding elements are not aligned as [31] did in 2D problems. The jump displacements are constant into the element, although there are others formulation which consider linear jumps inside such as [2] and [6].

3 CONSTITUTIVE MODEL

The discrete damage model for concrete, considering different threshold values under tension and compression is defined by the following equations:

$$
\begin{array}{ll}
\text{Discrete free energy density} & \phi\left(\left[\left|\mathbf{u}\right|\right],\bar{\alpha}\right)=\left(1-\omega\right)\phi_0\left(\bar{\alpha}\right),\begin{cases}\phi_0\left(\left[\left|\mathbf{u}\right|\right]\right)=\frac{1}{2}\left[\left|\mathbf{u}\right|\right]\cdot\mathbf{Q^e}\cdot\left[\left|\mathbf{u}\right|\right]\\ \mathbf{Q^e}=\mathbf{n}\cdot\mathbf{C}\cdot\mathbf{n}\end{cases}\\
\text{Constitutive equation} & \mathbf{T}=\frac{\partial\phi\left(\left[\left|\mathbf{u}\right|\right],\bar{\alpha}\right)}{\partial\left[\left|\mathbf{u}\right|\right]}=(1-\omega)\mathbf{Q^e}\cdot\left[\left|\mathbf{u}\right|\right]\\
\text{Damage variable} & \omega=1-\frac{\bar{q}(\bar{\alpha})}{\bar{\alpha}};\ \ \omega\in\left[-\infty,1\right]\\
\text{Evolution law} & \dot{\bar{\alpha}}=\dot{\bar{\lambda}}=\frac{\partial}{\partial t}\left(\bar{\alpha}\right),\ \ \bar{\alpha}\in\left[0,\infty\right]\\
\text{Damage criterion} & f(\mathbf{T},\bar{q})=\tau_{\mathbf{T}}-\bar{q};\ \ \tau_{\mathbf{T}}=\left\|\mathbf{T}\right\|_{\mathbf{Q^{e-1}}}=\sqrt{\mathbf{T}\cdot\mathbf{Q^{e-1}}\cdot\mathbf{T}}\\
\text{Hardening rule} & \dot{\bar{q}}\left(\bar{\alpha}\right)=\bar{H}\,\dot{\bar{\alpha}};\quad \bar{H}=\bar{q}^{'}\left(\bar{\alpha}\right)\le 0\\
\text{Loading-unloading conditions} & f\le 0;\quad \bar{\lambda}\ge 0;\quad \bar{\lambda}f=0;\quad \bar{\lambda}\dot{f}=0\ \text{(consistency)}
\end{array}
\tag{26}
$$

where ϕ is the discrete free energy density, $\mathbf{T}$ is the traction vector. The damage variable ω is defined in terms of the hardening/softening variable $\dot{\bar{q}}$, which is dependent on the hardening/softening parameter. The damage multiplier $\bar{\lambda}$ determines the loading-unloading conditions, the function $f(\mathbf{T},\bar{q})$, bounds the elastic domain defining the damage surface in the tractions space. The tangent constitutive equation, in terms of rates from the model in Eq. (26), is:

$$\dot{\mathbf{T}}=\mathbf{C}_d^T\cdot\left[\left|\dot{\mathbf{u}}\right|\right] \tag{27}$$

where $\mathbf{C}_d^T$ is the tangent constitutive operator, relating the traction and the jump displacement of the nonlinear loading interval, which is defined by

$$\mathbf{C}_d^T=\left(1-\omega\right)\mathbf{Q^e}-\frac{\bar{q}-\bar{H}\bar{\alpha}}{\bar{\alpha}^3}\left(\mathbf{Q^e}\cdot\left[\left|\mathbf{u}\right|\right]\otimes\left[\left|\mathbf{u}\right|\right]\cdot\mathbf{Q^e}\right) \tag{28}$$

and for the elastic loading and unloading interval ($\dot{d}=0$ and $\dot{\omega}=0$):

$$\mathbf{C}_d^T=\left(1-\omega\right)\mathbf{Q^e} \tag{29}$$

4 NUMERICAL EXAMPLES

In the three presented examples, the reinforcement was meshed with 3D linear elements with two nodes, which have three degrees of freedom each. The constitutive behavior of the steel reinforcement was modeled with a plasticity model with hardening. The steel elements were placed on the boundary of the solid elements, coupling the degree of freedom of both kinds of elements and then perfect bond was considered. Perfect bonding between steel bars and concrete was throughout assumed, as the failure of this type of slabs occurs mainly on flexure without evidence of debonding.

The model of finite elements with embedded discontinuities and the assumed constitutive behavior are validated by the numerical replication of the experimental results reported by [13]. The test specimen, shown in Figure 3a, was a square slab of sides 1.829 m long and a thickness 0.044 m. The vertical loads were applied at the top of the slab using four jacks with loading trees distributed to 16 load plates, as shown in Figure 3b. The mechanical properties for the concrete were: Young´s modulus E_c=19.90 GPa, Poisson ratio υ=0.2, ultimate tensile strength f_{tu}=3.1026 MPa, ultimate compressive strength f_{uc}=31.026 MPa and fracture energy

density G_f=0.098 N/mm and for the reinforcing steel: Young´s modulus E_s=206 GPa, Poisson ratio υ=0.3, yield stress σ_y=330.95 MPa and hardening modulus H=2.871GPa.

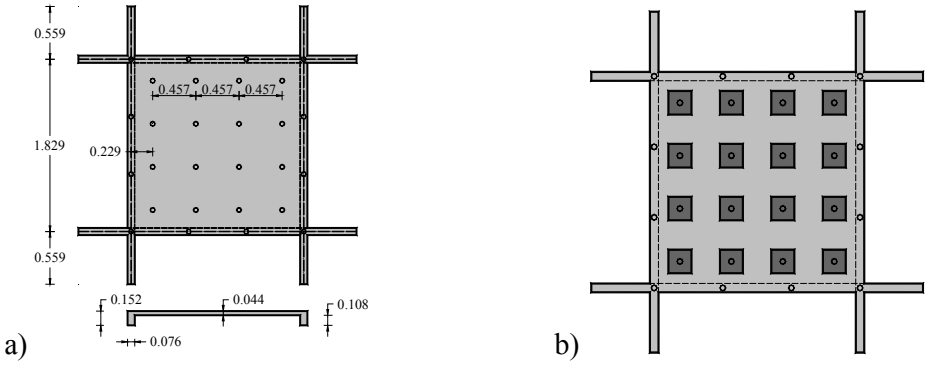

Figure 3: Experimental test: a) geometry and applied loads (adapted from [13])

The load *vs*. displacement at the center of the span curves are shown in Figure 4. These curves show numerical results congruent with the experimental reported by [13], both showing ultimate loading different to that calculated using the yield line theory.

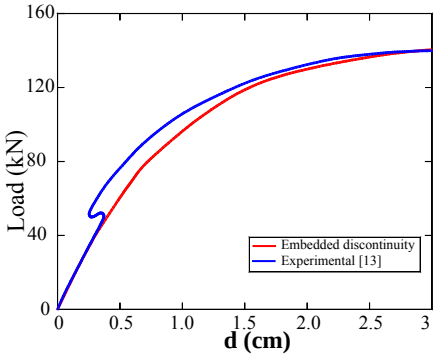

Figure 4: Comparison between experimental and numerical results

Two other slabs of square and rectangular geometry were also analyzed, 4x4m and 2x4m; both slabs were 10 cm thick and subjected to increasing uniform distributed loading. Two boundary conditions were considered: simply supported and fully fixed. As reinforcement, 3/8 in diameter steel bars spaced 20 cm in both orthogonal directions were used as shown in Figure 5. For both slabs, the plots of distributed load intensity *vs*. displacements at the center of the spans are shown in Figure 6. Here, it may be observed that for equal displacements, the intensities of the distributed loading for the fixed slabs are approximately five times larger than for the simple supported slabs.

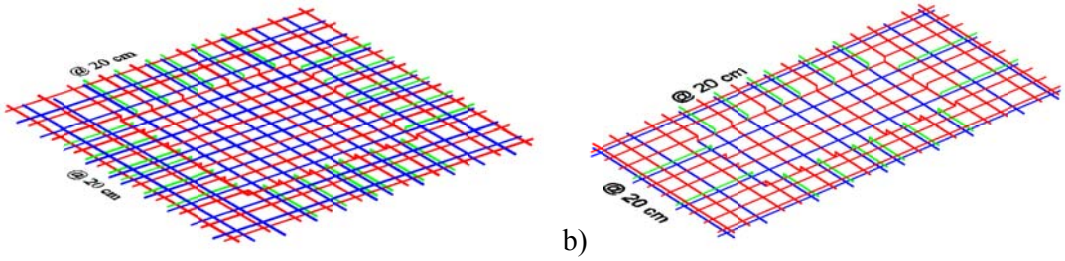

a) b)

Figure 5: Steel reinforcement of slabs: a) square and b) rectangular

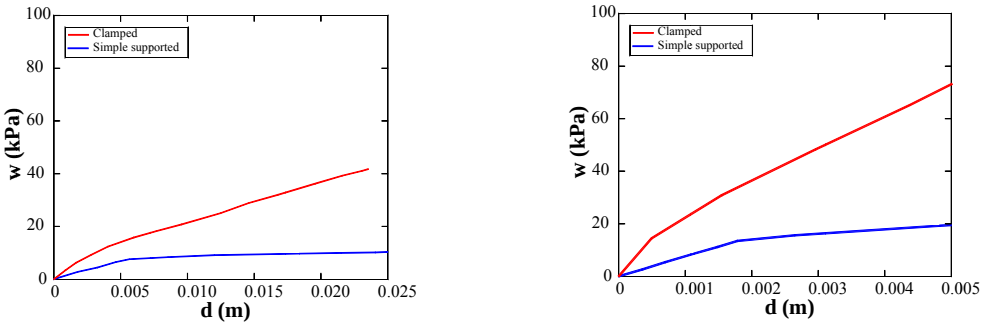

a) b)

Figure 6: Distributed load *vs.* displacement in: a) square slab and b) rectangular slab

In the fixed square slab, cracking simultaneously started on the top surface of the borders, growing to the center until a ring is formed, as shown in Figure 7a, whereas on the bottom surface, cracking paths form a kind of cross growing to both the corners and the borders, as shown in Figure 7b. In the simple supported condition, cracking started on the bottom surface at the corners and at the center, growing as shown in Figure 8b, whereas on top surface, it started at the corners, growing to the center, as shown in Figure 8a.

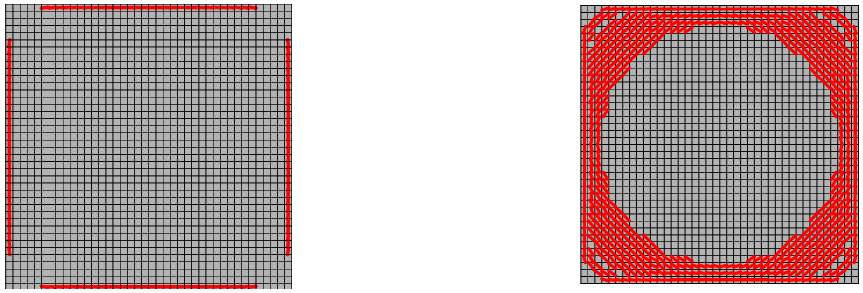

a)

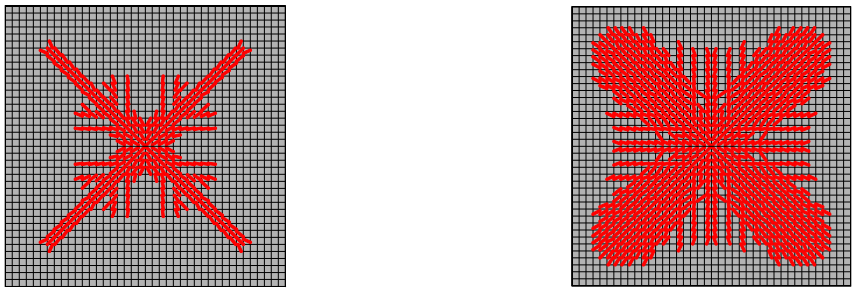

b)

Figure 7: Cracking propagation of a fixed square slab on the: a) top and b) bottom surface

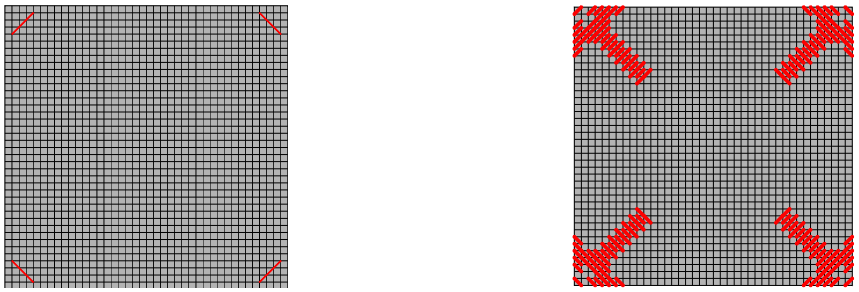

a)

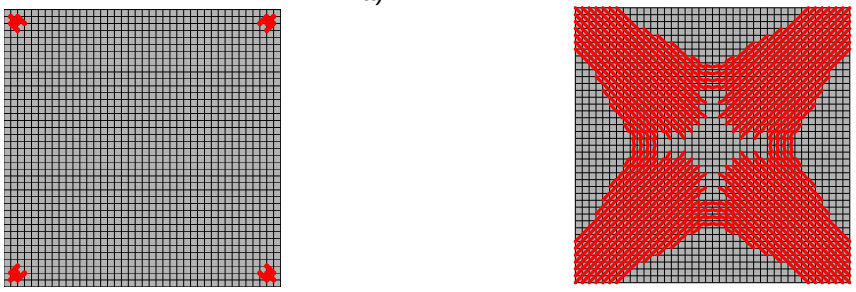

b)

Figure 8: Cracking propagation of a simple supported square slab on the: a) top and b) bottom surface

In the fixed rectangular slabs, cracking simultaneously started on the top surface along its large borders. Then, cracking appeared along its short borders, growing to the center until a ring is formed as shown in Figure 9a. On the bottom surface of the slab, cracking started along a strip at the center, parallel to the long borders, growing to the corners and the borders, as shown in Figure 9b. In the simple supported slab, cracking started along a strip at the center, parallel to the long borders as shown in Figure 10a; some cracks appeared on the top surface at the corner of the slabs as shown in Figure 10b. The cracking paths on the bottom surface of the slab are similar to the obtained with the yield line theory as well as the experimental results reported by [4].

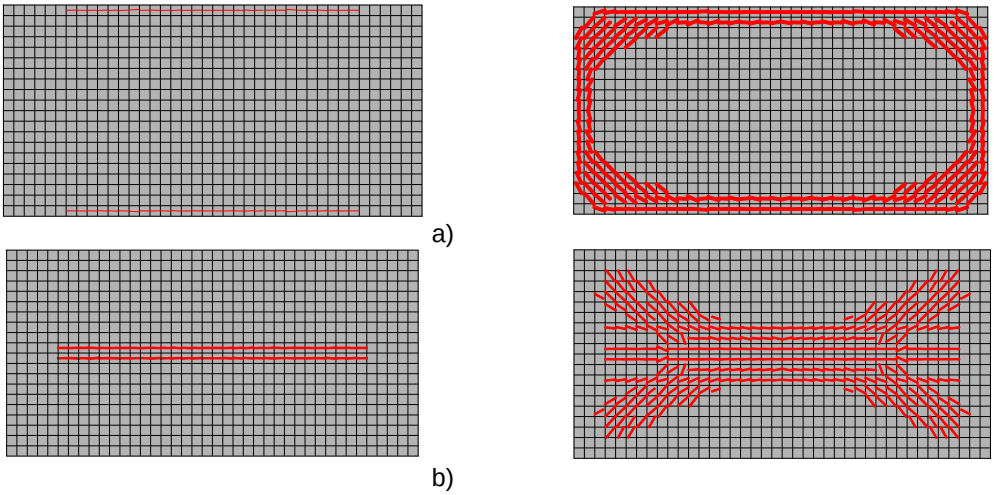

Figure 9: Cracking propagation of a fixed rectangular slab on the: a) top and b) bottom surface

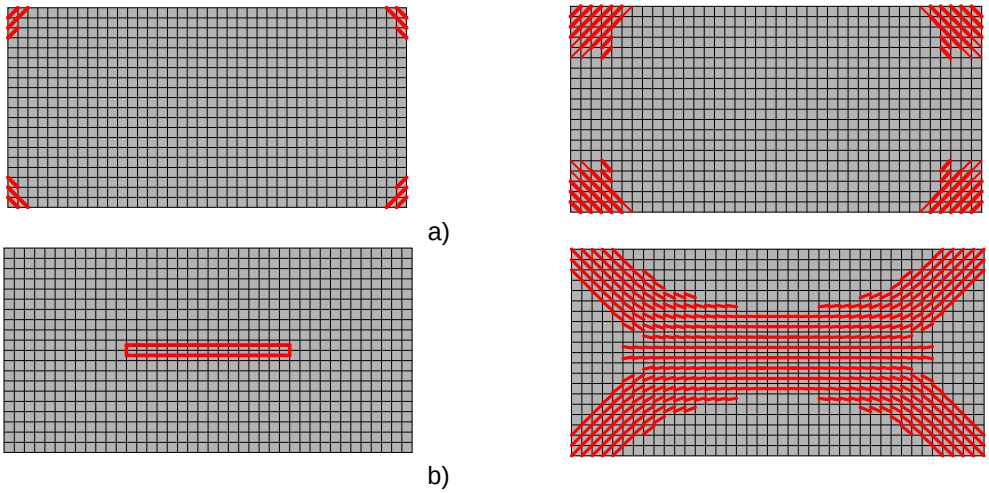

Figure 10: Cracking propagation of a simple supported rectangular slab on the: a) top and b) bottom surface

5 CONCLUSIONS

The coupling of solid elements with embedded discontinuities and bar elements is validated with the comparison of the load *vs* displacement curve between the numerical results and the reported in the literature. Although the experimental curve shows a recovery of the displacement, it is considered that it was a result of a slipping of the measurement equipment, as under an increasing vertical load it is not possible a recovery of the displacement at the center of the span.

ACKNOWLEDGES

The first author acknowledges the support given by the Universidad Autónoma Metropolitana and the financial support by CONACYT under the agreement number I010/176/2012, in the context of the research project: “Analysis and design of concrete slabs”.

The second author acknowledges the sponsorship by the General Directorate of Academic Personnel Affairs of UNAM of the PAPIIT project IN108512.

REFERENCES

[1] ABAQUS. Example problems manual, Volumen1: static and dynamic analysis. Version 6.11, E.U.A., (2011), p.881.

[2] Alfaiate, J., Simone, A. and Sluys, L.J. Non-homogeneous displacement jumps in strong embedded discontinuities. *Int. J Solids Struct.* (2003) **40**(21):5799-5817.

[3] ANSYS. ANSYS User's Manual version 13.0, ANSYS, Inc., Canonsburg, Pennsylvania, USA (2010).

[4] Bach, C. and Graf, O. Versuche mit allseitig aufliegenden, quadratischen and rechteckigen eisenbetonplatten. Deutscher Ausschuss für Elsenbeton (1915), 30, Berlin. (In German)

[5] Casadei, P., Parretti, R., Nanni, A. and Heinze, T. In situ load testing of parking garage reinforced concrete slabs: comparison between 24 h and cyclic load testing. *Practice Periodical on Structural Design and Construction, ASCE* (2005) **10**(1):40-48.

[6] Contrafatto, L., Cuomo, M., Di Venti, G.T. Finite Elements with non-homogeneous embedded discontinuities. In: 6th European Congress on Computational Methods in Applied Sciences and Engineering, ECCOMAS 2012, Vienna, Austria (2012).

[7] de Borst, R. and Nauta, P. Non-orthogonal cracks in a smeared finite element model. *Eng. Computations* (1985) **2**(1):35-46.

[8] DIANA. DIANA 9.0: Finite Element Analysis User's Manual Release. TNO DIANA BV, Delft, Holanda (2008).

[9] Foster, S.J., Bauley, D.G., Burgess, I.W. and Plank, R.J. Experimental behaviour of concrete floor slabs at large displacements. *Eng. Struc.* (2004) **26**:1231-1247.

[10] Galati, N., Nanni, A., Tumialan, J.G. and Ziehl, P.H. In-situ evaluation of two concrete slab systems, I: load determination and loading procedure. *J. Perform. Constr. Fac.-ASCE*, (2008) **22**(4):207-216.

[11] Gamble, W.L, Sozen, M.A. and Siess, C.P. An experimental study of a two-way floor slab. Structural Research Series No. 211, Department of Civil Engineering, University of Illinois (1961), p. 326.

[12] Gilbert, R.I. and Warner, R.F. Tension stiffening in reinforced concrete slabs. *J. Struct. Div.-ASCE* (1978) **104**(12):1885-1900.

[13] Girolami, A.G., Sozen M.A. and Gamble, W.L. Flexural strength of reinforced concrete slabs with externally applied in-plane forces. Report to the Department of Defense, Illinois University, Urbana, Illinois, (1970).

[14] Hand, F.D., Pecknold, D.A. and Schnobrich, W.C. Nonlinear analysis of reinforced concrete plates and shells. *J. Struct. Div.-ASCE* (1973) **99**(7):1491-1505.

[15] Hatcher, D.S., Sozen, M.A and Siess, C.P. An experimental study of a quarter-scale reinforced concrete flat slab floor. Structural Research Series No. 200, Department of Civil Engineering, University of Illinois (1960), p. 288.

[16] Hatcher, D.S., Sozen, M.A. and Siess C.P. A study of tests on a flat plate and a flat slab. Structural Research Series No. 217, Department of Civil Engineering, University of Illinois (1961), p. 504.

[17] Hinton, E., Abdel Rahman, H.H. and Zienkiewicz, O.C., Computational strategies for

reinforced concrete slab systems. International Association of Bridge and Structural Engineering, Colloquium on Advanced Mechanics of Reinforced Concrete (1981): 303-313.

[18] Jirsa, J.O., Sozen, M.A. and Siess, C.P. An experimental study of a flat slab floor reinforced with welded wire fabric. Structural Research Series No. 248, Department of Civil Engineering, University of Illinois (1962), p. 188.

[19] Jofriet, J.C. and McNeice, G.M. Finite element analysis of RC slabs. *J. Struct. Div.-ASCE*, (1971) **97**(3):785-806.

[20] Juárez, G., and Ayala, G. Variational formulation of the material failure process in solids by embedded discontinuities model. *Numer. Methods Partial Differ. Equ.* (2009) **25**(1):26-62.

[21] Juárez-Luna, G. and Ayala, G.A. Improvement of some features of finite elements with embedded discontinuities. *Eng. Fract. Mech.* (2014) **118**:31-48

[22] Juárez-Luna G. and Caballero-Garatachea O. Determinación de coeficientes de diseño y trayectorias de agrietamiento de losas aisladas circulares, elípticas y triangulares. Ingeniería Investigación y Tecnología (2014) **XV**(1):103-123. (In spanish)

[23] Kabele, P., Cervenka, V. and Cervenka, J. ATENA Program Documentation. Example Manual. ATENA Engineering (2010), p. 90.

[24] Kupfer, H.B. and Gerstle, K.H. Behavior of concrete under biaxial stresses. *J. Eng. Mech. -ASCE* (1973) **99**(4):853-866.

[25] Kwak, H.G. and Filippou, F.C. Finite element analysis of reinforced concrete structures under monotonic loads", Department of Civil Engineering, University of California, Berkeley, California (1990), p. 124.

[26] Lin, C.S. and Scordelis, A.C. Nonlinear analysis of RC shells of general form. *J. Struct. Div.-ASCE* (1975) **101**(3):523-238.

[27] Lotfi, HR, Shing, P. Embedded representation of fracture in concrete with mixed finite elements. *Int. J. Numer. Methods Eng.* (1995) **38**(8):1307-1325.

[28] Mayes, G.T., Sozen, M.A. and Siess, C.P. Tests on a quarter-scale model of a multiple-panel reinforced concrete flat plate floor. Structural Research Series No. 181, Department of Civil Engineering, University of Illinois (1959).

[29] Mcneice, A.M. (1967), "Elastic-plastic bending of plates and slabs by the finite element method", Dissertation, London University.

[30] Rots, J.G. (1988), "Computational modeling of concrete fracture , Dissertation, Delft University of Technology, The Netherlands, p.132.

[31] Sancho, J.M., Planas, J., Cendón, D.A., Reyes, E., Gálvez, J.C. An embedded crack model for finite element analysis of concrete fracture. *Eng. Fract. Mech.* (2007) **74**(1-2):75-86.

[32] Smadi, M.M. and Belakhdar, K.A. Development of finite element code for analysis of reinforced concrete slabs. *Jordan J. Civ. Eng.* (2007) **1**(2):202-219.

[33] Taylor, L.R. A finite element analysis program (FEAP) v8.2. Department of Civil and Environmental Engineering, University of California at Berkeley, Berkeley, CA (2008).

[34] Vanderbilt, M.D., Sozen, M.A. and Siess, C.P. An experimental study of a reinforced concrete two-way floor slab with flexible beams. Structural Research Series No. 228, Department of Civil Engineering, University of Illinois, (1961), p. 188.

[35] Wang Y., Dong Y. y Zhou G. Nonlinear numerical modeling of two-way reinforced

concrete slabs subjected to fire. *Comput. Struct.* (2013) **119**(1):23-36.

[36] Wells, G.N. and Sluys, L.J. A new method for modelling cohesive cracks using finite elements. *Int. J. Numer. Methods Eng.* (2001) **50**(12):2667-2682.

[37] Westergaard, H.M. and Slater, W.A. Moments and stresses in slabs. *Proc. of the American Concrete Institute* (1921) **17**(2): 415-538.